

Secondary Organic Aerosol formation from isoprene photooxidation during cloud condensation-evaporation cycles

L. Brégonzio-Rozier¹, C. Giorio^{2,3}, F. Siekmann⁴, E. Pangui¹, S. B. Morales¹, B. Temime-Roussel⁴, A. Gratien¹, V. Michoud¹, M. Cazaunau¹, H. L. DeWitt⁴, A. Tapparo³, A. Monod⁴ and J.-F. Doussin¹

[1]{Laboratoire Interuniversitaire des Systèmes Atmosphériques (LISA), UMR7583, CNRS, Université Paris-Est-Créteil (UPEC) et Université Paris Diderot (UPD), Institut Pierre Simon Laplace (IPSL), Créteil, France }

[2]{Department of Chemistry, University of Cambridge, Cambridge CB2 1EW, U.K. }

[3]{Dipartimento di Scienze Chimiche, Università degli Studi di Padova, Padova, 35131, Italy }

[4]{Aix-Marseille Université, CNRS, LCE FRE 3416, 13331, Marseille, France }

Correspondence to: L.Brégonzio-Rozier (lola.bregonzio@lisa.u-pec.fr) and A. Monod (anne.monod@univ-amu.fr)

Abstract

The impact of cloud events on isoprene secondary organic aerosol (SOA) formation has been studied from an isoprene/NO_x/light system in an atmospheric simulation chamber. It was shown that the presence of a liquid water cloud leads to a faster and higher SOA formation than under dry conditions. When a cloud is generated early in the photooxidation reaction, before any SOA formation has occurred, a fast SOA formation is observed with mass yields ranging from 0.002 to 0.004. These yields are two and four times higher than those observed under dry conditions. When the cloud is generated at a later photooxidation stage, after isoprene SOA is stabilized at its maximum mass concentration, a rapid increase (by a factor of two or higher) of the SOA mass concentration is observed. The SOA chemical composition is influenced by cloud generation: the additional SOA formed during cloud events is composed of both organics and nitrate containing species. This SOA formation can be linked to water soluble volatile organic

1 compounds (VOCs) dissolution in the aqueous phase and to further aqueous phase reactions.
2 Cloud-induced SOA formation is experimentally demonstrated in this study, thus highlighting
3 the importance of aqueous multiphase systems in atmospheric SOA formation estimations.
4

5 **1 Introduction**

6 Tropospheric fine aerosol particles are known to cause several environmental impacts,
7 including adverse health effects and radiative forcing on climate (Hallquist et al., 2009; IPCC,
8 2013). Organic compounds contribute a significant percentage (from 20 to 90 %) of the total
9 submicron aerosol mass and secondary organic aerosol (SOA) accounts for a substantial
10 fraction of this organic mass (Kanakidou et al., 2005; Zhang et al., 2007). SOA formation results
11 from the atmospheric oxidation of volatile organic compounds (VOCs) leading to the formation
12 of less volatile oxidation products that can undergo gas to particle conversion. Some of these
13 oxidized species contain acid, hydroxyl and/or aldehyde functional groups that increase their
14 water solubility, and thus explain their presence in cloud droplets (Herckes et al., 2013;
15 Herrmann et al., 2015). Clouds cover ~ 70 % of the earth surface on average (Stubenrauch et
16 al., 2013; Wylie et al., 2005) and only ~ 10 % of them precipitate while the remaining ~ 90%
17 dissipate, leading to evaporation of volatile compounds and condensation of lower volatility
18 species (Herrmann et al., 2015).

19 In the aqueous phase, soluble organic compounds can react with hydroxyl radicals (OH) and/or
20 by direct photolysis, similar to reactions in the gas phase but in a depleted NO_x environment.
21 Aqueous-phase chemical pathways thus lead to enhanced production of acids, such as oxalic
22 acid, (Carlton et al., 2007; Carlton et al., 2006), and oligomers that have been observed from
23 the photooxidation of pyruvic acid (Reed Harris et al., 2014), glyoxal (Carlton et al., 2007),
24 methylglyoxal (Lim et al., 2013; Tan et al., 2012), methacrolein (MACR) and methyl vinyl
25 ketone (MVK) (Liu et al., 2012b), and glycolaldehyde (Perri et al., 2009). The produced
26 oligomers and/or *HUmic LIke Substances* (HULIS) are low volatility species and may remain
27 in the particle phase after water evaporation (Ervens et al., 2014; Lim et al., 2013), leading to
28 the formation of new SOA from aqueous phase, called aqSOA (Ervens et al., 2011).

29 Recent laboratory (Lim et al., 2013; Liu et al., 2012b), field (Dall'Osto et al., 2009; Huang et
30 al., 2006; Lee et al., 2012; Lin et al., 2010; Peltier et al., 2008) and modelling studies (Carlton
31 and Turpin, 2013; Couvidat et al., 2013; Ervens et al., 2008) suggest that this additional SOA
32 formation pathway can be considered important in terms of quantity (up to + 42 % of carbon

1 yields (Ervens et al., 2008)) and composition (Ervens et al., 2011), however these processes
2 have never been directly experimentally demonstrated.

3 Indeed, previous experiments from the literature evaluating an SOA source in the aqueous phase
4 were only carried out in homogeneous phases separately. Studies were performed in
5 homogeneous aqueous phase to observe oligomers and low volatility organic acids formation
6 (Altieri et al., 2008; Carlton et al., 2006; Liu et al., 2012b), in homogeneous aqueous phase
7 solutions with nebulization and drying of the solutions to evaluate aqSOA formation (El
8 Haddad et al., 2009; Ortiz-Montalvo et al., 2012), and in the gas phase with gasSOA formation
9 followed by immersion of these gasSOA in homogeneous aqueous phase (Bateman et al., 2011;
10 Liu et al., 2012a). Previous experimental studies have not been performed on a multiphase
11 system and, as a result, they only refer to the amount of precursor consumed in aqueous phase
12 to determine formation yields. Consequently, and contrary to SOA yields obtained in gaseous
13 phase (gasSOA), these yields cannot be directly implemented in multiphase models because the
14 link between aqueous and gaseous phases (transfer between the two phases) is not taken into
15 account. These works thus lead generally to an overestimation of yields associated with gaseous
16 precursors, whose concentrations depend on the relative importance of their loss in the gaseous
17 phase and their transfer in the aqueous phase. Furthermore, Daumit et al. (2014) recently
18 showed that the reactivity in a multiphase system may be substantially different from reactivity
19 in homogeneous aqueous phase, highlighting the need to study controlled multiphase systems,
20 which are more realistic for the atmosphere.

21 In the present study, taking advantage of the ability to artificially produce clouds in the CESAM
22 simulation chamber (Wang et al., 2011), dedicated multiphase experiments were carried out to
23 study SOA multiphase formation from isoprene in order to experimentally observe and quantify
24 the impact of cloud-phase reactions on SOA formation. Isoprene was chosen as the precursor
25 because it is highly reactive and it represents the most emitted VOC globally. Isoprene gas-
26 phase oxidation is known to lead to low yields of gasSOA (Brégonzio-Rozier et al., 2015;
27 Dommen et al., 2006; Edney et al., 2005; Kleindienst et al., 2006; Kroll et al., 2005; Zhang et
28 al., 2011) and to large amounts of volatile water soluble compounds (such as methylglyoxal,
29 glyoxal, glycolaldehyde and pyruvic acid) which can interact with the aqueous phase in the
30 atmosphere and potentially lead to the formation of aqSOA after water evaporation. In this
31 study, the formation of aqSOA from isoprene photooxidation in the presence of clouds is

1 investigated by studying the concentration and chemistry of gaseous, aqueous and particulate
2 phases, and the chemical exchanges between these phases.

3

4 **2 Experimental section**

5 Experiments were carried out in the CESAM chamber as described in detail by Wang et al.
6 (2011), and Brégonzio-Rozier et al. (2015). Briefly, it is a 4.2 m³ stainless steel reactor equipped
7 with three xenon arc lamps and Pyrex[®] filters of 6.5 mm thickness. During each experiment,
8 the reactive mixture is maintained at a constant temperature with a liquid coolant circulating
9 inside the chamber double wall and monitored by a thermostat (LAUDA, Integral T10000 W).
10 Temperature and relative humidity (RH) are continuously monitored in the chamber using a
11 Vaisala HUMICAP HMP234 probe.

12 **2.1 Experimental protocols**

13 **2.1.1 Cloud generation**

14 To investigate the influence of a cloud on SOA formation, a specific protocol allowing cloud
15 generation with a lifetime close to droplet lifetime in the atmosphere (~ 2-30 minutes, Colvile
16 et al. (1997)) in the presence of light was designed. Clouds were generated by adding water
17 vapour into the chamber up to saturation: at 22°C, ca. 81 g of water vapour was introduced to
18 reach saturation and to observe cloud formation. The ultrapure water used was obtained fresh
19 from an Elga Stat Maxima Reverse Osmosis Water Purifier system, which includes reverse
20 osmosis, micro-filtration, nuclear-grade deionization, activated carbon modules and an
21 irradiation module at 254 nm leading to a resistivity greater than 18.2 MΩ. As described in
22 detail by Wang et al. (2011), water vapour was pressurized in a 5 L small-stainless steel vessel
23 located below the chamber. This small reactor was filled halfway with ultrapure water and
24 heated to reach a relative pressure of 1000 mbar. Half-inch stainless steel tubing equipped with
25 a valve was used to connect the vessel to the chamber and allowed water vapour injection near
26 the chamber's fan. Due to the 1000 mbar pressure difference between the small reactor and the
27 chamber, opening the valve induced an instantaneous adiabatic cooling of the water vapour in
28 the chamber. Prior to injection in the chamber, the pressurized reactor was purged at least five
29 times to eliminate any residual air. Using this procedure, starting from dry conditions in the
30 chamber (< 5 % RH), the first water vapour injection allowed the chamber to reach 80 % RH

1 within less than one minute. A second water vapour injection leads to water saturation in the
2 chamber and cloud formation. The obtained clouds were monitored, and Table 1 shows that
3 their mean physical properties were close to those of typical atmospheric clouds. A typical
4 droplet mass size distribution is also shown in Figure S1. Using the above described procedure,
5 several clouds could be generated during one experiment (typically 2 or 3).

6 **2.1.2 Cleaning and control experiments**

7 In order to avoid any contamination from semi-volatile organic compounds (SVOCs) off-
8 gassing from the walls, a manual cleaning of the chamber walls was performed prior each
9 experiment. To this purpose, lint free wipes (Spec-Wipe[®] 3) soaked in ultrapure water (18.2
10 MΩ, ELGA Maxima) were used. To complete this manual cleaning, the walls were heated at
11 40°C and the chamber was pumped down to secondary vacuum in the range of 6×10^{-4} mbar
12 for two hours at a minimum. After pumping, the chamber was cooled down to 20-22°C, and a
13 control experiment was performed by generating a cloud in the presence of a N₂/O₂ mixture (80
14 % / 20 %), under irradiation. All of the instruments were connected to the chamber during the
15 entire control experiment which lasted for ~ one hour after cloud generation. The aim of these
16 control experiments was to monitor aqSOA formation arising from the dissolution of any
17 remaining water soluble VOCs off-gassing from the walls or from contaminants introduced
18 with water vapour. After this control experiment, the temperature of the chamber walls was
19 increased to 50°C before starting overnight pumping. The amount of particulate matter
20 observed during all the control experiments was fairly reproducible with an average value of
21 $1.5 \pm 0.4 \mu\text{g m}^{-3}$ of dried particles formed during a cloud event (Table S1).

22 **2.1.3 Cloud experiments**

23 Two types of cloud experiments were performed to study the impact of clouds on isoprene-
24 SOA formation: i) clouds generated during the first stages of isoprene photooxidation, prior any
25 gasSOA formation; and ii) clouds generated during later stages of the reaction, when gasSOA
26 mass reached its maximum. For each type of experiment, the protocol followed before
27 beginning irradiation was the same as the one described in Brégonzio-Rozier et al. (2015). After
28 overnight pumping, synthetic air was injected into the chamber to reach atmospheric pressure.
29 This air was comprised of approximately 80 % N₂, produced from the evaporation of
30 pressurized liquid nitrogen, and around 20 % O₂ (Linde, 5.0). A known pressure of isoprene,
31 leading to a mixing ratio of 800-850 ppb in the chamber, was then introduced using a known

1 volume glass bulb. Nitrous acid (HONO) was used as the OH source. HONO was produced by
2 adding sulfuric acid (10^{-2} M) dropwise into a solution of NaNO_2 (0.1 M) and flushed into the
3 chamber using a flow of N_2 . NO_x was also introduced as a side product during HONO injection.
4 Photooxidation of the system was then initiated by turning on the lamps (reaction time 0
5 corresponds to the irradiation start). Table 2 shows all of the experimental initial conditions,
6 the number of generated clouds during each experiment and their maximum liquid water
7 contents (LWC_{max}) for both types of experiments.

8 In the first type of experiment, a diphasic system (gas-cloud), the aim was to produce evapo-
9 condensation cycles in the presence of gaseous isoprene oxidation products prior to any
10 gasSOA formation. This type of experiment started under dry conditions ($< 5\%$ RH), and the
11 first water vapour injection, leading to $\sim 80\%$ RH, was performed after 2 hours of irradiation.
12 This time corresponded to $\sim 80\%$ of isoprene consumption and to the maximum concentration
13 of the first generation isoprene gaseous reaction products (Brégonzio-Rozier et al., 2015). After
14 ca. ten minutes, the second water vapour injection, allowing cloud formation by saturation, was
15 made. Two to three clouds were generated during each diphasic experiment (gas-cloud).

16 In the second type of experiment, a triphasic system (gas-SOA-cloud), we tested the influence
17 of cloud generation on isoprene photooxidation during a later stage of the reaction, i.e., when
18 the first generation oxidation gaseous products of isoprene were mostly consumed, and when
19 maximum gasSOA mass concentration was reached. In this case, in addition to the dissolution
20 of gaseous species in the aqueous phase, some of the condensed matter could also dissolve in
21 droplets. In this type of experiment, the formation of gasSOA was monitored under dry
22 conditions ($< 5\%$ RH), and the first cloud was generated when the maximum gasSOA mass
23 concentration was reached, generally after 7 to 9 hours of irradiation, in a system containing
24 more oxidized species than in the diphasic system. One to two clouds were generated during
25 each triphasic experiment (gas-SOA-cloud). The variation of species under dry conditions for
26 triphasic experiments presented here can be seen in Brégonzio-Rozier et al. (2015).

27 **2.2 Measurements**

28 A Fourier Transform Infra-Red spectrometer (FTIR, Bruker[®], TENSOR 37) was used to
29 measure concentrations of isoprene, MVK, MACR, formaldehyde, methylglyoxal,
30 peroxyacetyl nitrate (PAN), formic acid, carbon monoxide (CO) and NO_2 during dry
31 conditions. Complementary to FTIR measurements, a proton-transfer time of flight mass

1 spectrometer (PTR-ToF-MS 8000, Ionicon Analytik®) was used for online gas-phase
2 measurements in the m/z range 10–200 including isoprene, the sum of MACR and MVK, 3-
3 methylfuran (3 M-F), acetaldehyde, the sum of glycolaldehyde and acetic acid, acrolein,
4 acetone, hydroxyacetone, and a few other oxygenated VOCs (de Gouw et al., 2003a). The PTR-
5 ToF-MS was connected to the chamber through a 120 cm long Peek™ capillary heated at
6 100°C. Its signal was calibrated using a certified gas standard mixture (EU Version TO-14A
7 Aromatics 110L, 100 ppbV each). Considering the high amounts of water in the sampled air
8 during and after cloud events, the sum of the primary H_3O^+ and cluster ion $\text{H}_2\text{O}\cdot\text{H}_3\text{O}^+$ signal
9 derived from $\text{H}_3^{18}\text{O}^+$ (m/z 21.023) and $\text{H}_2^{18}\text{O}\cdot\text{H}_3\text{O}^+$ (m/z 39.033) count rate was taken into
10 account for quantification (de Gouw and Warneke, 2007; de Gouw et al., 2003b; Ellis and
11 Mayhew, 2014). A commercial UV absorption monitor (Horiba®, APOA-370) was used to
12 measure ozone. NO was monitored by a commercial chemiluminescence NO_x analyser
13 (Horiba®, APNA-370). During humid conditions, the NO_2 signal from the NO_x monitor was
14 used to determine NO_2 mixing ratios, a correction was applied to take into account interferences
15 due to the presence of NO_y during the experiments (Dunlea et al., 2007). An instrument
16 developed in-house (NitroMAC), based on the wet chemical derivatization technique and
17 HPLC-VIS detection (Zhou et al., 1999) and described in detail by Michoud et al. (2014), was
18 used to measure nitrous acid (HONO).

19 Aerosol size distribution from 10.9 to 478 nm, total number and volume concentration of the
20 particles were measured by a Scanning Mobility Particle Sizer (SMPS). This instrument
21 includes a Differential Mobility Analyzer (DMA, TSI, model 3080) coupled with a
22 Condensation Particle Counter (CPC, TSI, model 3010). A high resolution time-of-flight
23 aerosol mass spectrometer (HR-ToF-AMS, Aerodyne) was used to measure chemical
24 composition of non-refractory particulate matter, such as organics, nitrate and ammonium
25 (Canagaratna et al., 2007; De Carlo et al., 2006). The HR-ToF-AMS was used under standard
26 operating conditions (vaporizer at 600°C and electron ionization at 70 eV). Standard AMS
27 calibration procedures using ammonium nitrate particles performed regularly, including the
28 Brute Force Single Particle (BFSP) ionization efficiency calibration and size calibration. For
29 HR-ToF-AMS data analysis, Squirrel (ToF-AMS Analysis 1.51H) and PIKA (ToF-AMS HR
30 Analysis 1.10H) packages for the software IGOR Pro 6.21 were used. The ionization efficiency
31 obtained during BFSP calibration was used to calculate mass and standard adjustments were
32 used to account for the relative ionization efficiency of each class of compounds (nitrate,
33 sulfate, ammonium, and organics) (Canagaratna et al., 2007). The standard fragmentation table

1 was adjusted to correct for the corrected air fragment column for the carrier gas. A collection
2 efficiency of 0.5 was used for the organics to adjust for particle bounce at the heater
3 (Middlebrook et al., 2012).

4 The SMPS and the HR-ToF-AMS were connected to the chamber through the same sampling
5 line and dried with a 60 cm Nafion[®] tube (Permapure[™], model MD-110). The relative humidity
6 was continuously measured after drying and was never above 22 % RH at the outlet of the
7 Nafion[®] tube. Systematically maintaining the relative humidity in the sampling line lower than
8 the efflorescence point of any expected particulate matter was a critical parameter to effectively
9 detect additional SOA and not a water uptake due to the change in relative humidity in the
10 chamber. It is hence important to consider that all the SOA quantity, size distribution or AMS
11 analysis discussed later in this paper concern dried SOA.

12 The size distributions of cloud droplets were determined by a white light optical particle counter
13 (Welas[®] 2000, Palas) using the refractive index of water (1.33+0i). The particle size range of
14 this sensor was 0.6-40 μm . The Welas optical particle counter was calibrated using a calibration
15 dust (CalDust 1100) exhibiting the same index of refraction as polystyrene latex (PSL) spheres.

16

17 **3 Results and discussion**

18 The aim of these experiments was to evaluate the influence of clouds on SOA formation in the
19 isoprene/NO_x/air/light system. This system was already characterized in detail under dry
20 conditions in the same chamber by Brégonzio-Rozier et al. (2015). To that purpose, as stated
21 above, two new protocols were tested: a diphasic and a triphasic system. The corresponding
22 results are shown in Figures 1 to 4, and discussed hereafter.

23 **3.1 SOA formation in the presence of a cloud**

24 During cloud events, a sudden and significant increase in dried SOA mass concentration was
25 observed in both types of experiments (Figure 1a and 1a'). This rise lasted from the outset of
26 the cloud generation until its evaporation, i.e., during the whole cloud event. Increases in SOA
27 mass concentrations for diphasic and triphasic experiments observed during cloud events are
28 presented in Table 3. During the first cloud of each experiment, an increase in mass ranging
29 from 3.9 to 8 $\mu\text{g m}^{-3}$ was observed for diphasic experiments, and from 4.3 to 7.2 $\mu\text{g m}^{-3}$ for
30 triphasic experiments, which is more than 3 times higher than the increase observed in control

1 experiments (Table S1). The additional SOA formation observed in diphasic and triphasic
2 experiments are called aqSOA formation hereafter. In triphasic experiments, no direct link
3 between mass concentration levels of gasSOA prior to cloud generation and the maximum value
4 reached by aqSOA during cloud events was observed. The comparison of triphasic and diphasic
5 experiments shows that the observed increase in SOA mass concentration was the same order
6 of magnitude, suggesting that the concentration, or even the initial presence of particulate phase
7 (gasSOA), had no significant influence on aqSOA formation. The comparison between diphasic
8 and triphasic experiments also suggests that the presence of a reacting mixture that underwent
9 more oxidation steps, and thus composed of more oxidized compounds did not play a significant
10 role in the amount of aqSOA produced.

11 The SOA mass size distributions (Figure 1b) show that, for the diphasic experiment D300113,
12 the mode of the distribution increased gradually during the first cloud event, with a maximum
13 mode around 225 nm just before cloud evaporation. For the triphasic experiment T280113
14 (Figure 1b'), the particle size distribution of the gasSOA formed under dry conditions increased
15 during the first minute of the first cloud event, then a second mode, with larger size, was formed.
16 While the initial mode showed no significant variation in size, the second mode increased in
17 size gradually until reaching a diameter of around 250 nm before cloud evaporation. A link
18 between high oxidation stage species and aqSOA formation cannot be highlighted in these
19 experiments due to the subsistence of the initial mode (corresponding to gasSOA) and the
20 systematic and reproducible formation of a second mode in all triphasic experiments. The
21 observation of such a growing second mode, called the "droplet mode", has been previously
22 underscored during field observations in the presence of water (Hering and Friedlander, 1982;
23 John et al., 1990; Meng and Seinfeld, 1994). This "droplet mode" is hypothesized to be formed
24 through volume-phase reactions in clouds and wet aerosols (Ervens et al., 2011) and has been
25 found to be significantly enriched in highly oxidized organics, nitrates and organosulfates
26 (Ervens et al., 2011).

27

28 For the subsequent clouds, smaller increases in SOA mass (from 1.9 to 5.1 $\mu\text{g m}^{-3}$ for diphasic
29 experiments, and from 2.1 to 5.5 $\mu\text{g m}^{-3}$ for triphasic experiments, as shown in Table 3) were
30 observed. No link between increases in SOA mass concentration and surface concentration of
31 cloud droplets was observed to explain this difference, so a smaller cloud droplet size and/or
32 lower water concentration was not the reason for these reduced aqSOA increases. However, it

1 could be due to shorter cloud lifetimes after the initial cloud generation (Table 3) since aqSOA
2 production stopped immediately after cloud evaporation in all experiments.

3 After cloud evaporation, the mode diameter and concentration of the measured distributions
4 slowly decayed (Figures 1a and 1a'). For diphasic experiments, the gradual decrease in
5 concentration lasted for 25 to 35 minutes before reaching a plateau with a value of ca. $0.6 \mu\text{g m}^{-3}$,
6 the same order of magnitude to that observed in control experiments (Figure S2). A decay
7 in SOA mass concentration was also observed after cloud evaporation for triphasic experiments.
8 This gradual decrease lasted for 20 min to 1 hour before reaching a stable SOA mass value
9 close to the one observed before cloud generation (T280113 and T130313) and to a value of
10 around $0.5\text{-}1 \mu\text{g m}^{-3}$ for experiments with lower initial gasSOA mass concentration (T160113
11 and T250313). This decrease in mass concentration was explained by a slow decay of the
12 second aerosol size mode which tended to disappear when a stabilization of SOA mass
13 concentrations was observed (Figures 1a' and 1b').

14 Figures 1b and 1b' show that, for both types of experiments (diphasic and triphasic systems),
15 this slow decay in SOA mass observed after cloud evaporation was due to the shrinkage of
16 particles, and was not linked to a direct particle wall loss effect. It seems that this decay was
17 due to wall re-partitioning of the SVOCs formed during the cloud event. Recently, it has been
18 shown that losses of semi-volatile species to chamber walls could affect SOA formation rates
19 during photooxidation experiments, due to a competition between condensation of SVOCs on
20 the walls and on particles (Loza et al., 2010; Matsunaga and Ziemann, 2010; Zhang et al., 2014).
21 SVOCs experience a continuous gas-wall partitioning in chambers, the extent of this effect
22 depending on the molecular structure of the compound, the wall material and the experiment's
23 organic loading, humidity and temperature. If production of additional semi-volatile species
24 occurs in the droplet during cloud events, Henry's Law equilibrium suggests that these species
25 are isolated from the walls in the droplets. After cloud dissipation, additional SOA mass is
26 formed from these SVOCs which, at the same time, also experience a re-partitioning between
27 particles and the walls. When the cloud is evaporated, since the available particle surface area
28 is around 400 times smaller than the geometric wall surface area, the additional SOA mass
29 decreases due to this equilibrium re-establishment under humid conditions. Wall loss kinetics
30 data reported in the literature for a Teflon chamber (Matsunaga and Ziemann, 2010) has led to
31 a characteristic time ranging from one hour for non-polar species to 8 minutes for carbonyls:
32 these results are compatible with the rates of the decays observed in our experiments (20 min

1 to one hour). Furthermore, pseudo-first order rates for loss processes of organic compounds
2 found in Wang et al. (2011) suggest that similar wall loss kinetics are expected in the CESAM
3 chamber.

4 Assuming that this observed SOA mass decay is due to wall re-partitioning, this process will
5 not occur in the atmosphere, and aqSOA production can be determined using the maximum
6 mass concentration measured at the end of each cloud event. In that case, aqSOA mass yield
7 from isoprene photooxidation in the presence of clouds would be between 0.002 and 0.004
8 considering our results from the diphasic experiments, or between two and four times higher
9 than mass yields observed for isoprene photooxidation experiments carried out under dry
10 conditions with preliminary manual cleaning (Brégonzio-Rozier et al., 2015). For triphasic
11 experiments, the observed increase of total SOA mass concentration at the end of each cloud
12 event was at least a factor of two compared to the gasSOA mass concentrations reached under
13 dry conditions prior cloud formation. Hence, it can be assumed that a substantial aqSOA
14 production was observed in both types of experiments. Furthermore, the fact that additional
15 SOA mass was formed in the triphasic system (i.e., in the second mode) seems to demonstrate
16 that the role of cloud chemistry is not just to increase the rate of gas-phase oxidation reactions
17 but is adding new chemistry.

18 **3.2 Dissolution and reactivity of gaseous species in cloud droplets**

19 The time profiles of the gas phase reactants and oxidation products during a diphasic experiment
20 are shown in Figure 2 (similar profiles were observed for triphasic systems, see Figure S3) in
21 which two clouds were generated. Ozone, NO_x and HONO showed no significant change in
22 their concentrations during cloud events (Figures 2b and 2c), with mixing ratios remaining at
23 around 5 ppbv for HONO and NO. The concentrations of isoprene, the sum of MACR and
24 MVK, acetone and C₅H₈O (compound that may be attributed to 2-methylbut-3-enal, Brégonzio-
25 Rozier et al. (2015)) also did not seem to be influenced by cloud generation (Figures 2a and 2f),
26 as their concentrations remained unchanged during cloud events. On the contrary, more water
27 soluble species (for example, methylglyoxal and formic acid) showed a sharp decrease in their
28 concentrations during cloud generation (Figures 2d, 2e, 2g and 2h). During each cloud event
29 and for 20 additional minutes, the PTR-ToF-MS signal was not used due to possible droplet
30 impaction in the heated sampling line. Using the concentrations of VOCs before each cloud
31 event (C_{before}) and 20 minutes after (C_{after}), we calculated the gas phase concentration changes

1 during cloud events ($\Delta C_{cloud} = C_{before} - C_{after}$, see Table 4). From these data, it can be noted that
2 the loss of the most water soluble VOCs (e.g., glycolaldehyde, acetic acid, methylglyoxal,
3 formic acid and hydroxyacetone) was significant during the cloud events (between 32 % and
4 52 %, see Table 4). Isoprene was excluded from this calculation as its gas phase photochemical
5 decay did not seem to be affected by the cloud events.

6 Following a hypothesis based on the kinetic determination of the mass-transport of VOCs from
7 the gas phase to water droplets (Schwartz, 1986), Henry's Law equilibrium was considered
8 immediate at the start of cloud generation. This hypothesis was used to estimate the theoretical
9 mass of individual VOCs transferred into the aqueous phase (see Supplement Sect. 1). The
10 estimation was done using the experimental data of each gaseous VOC concentration prior
11 cloud formation (C_{before}) and using the measured LWC. The obtained values are summed and
12 the total mass of VOCs theoretically transferred to the aqueous phase is compared to the mass
13 of formed aqSOA in Table 4. It can be considered that the estimated transferred mass represents
14 a lower limit since this calculation only considers the measured VOCs and thus neglects the
15 contribution of other undetected VOCs such as the organic nitrates or glyoxal (which should
16 contribute to an extent comparable to methylglyoxal or glycolaldehyde (Galloway et al. (2011)).
17 However, this lower limit is much higher than the maximum aerosol mass concentration
18 increase observed during cloud events by more than an order of magnitude. This result thus
19 suggests that, even if a small part of this dissolved organic matter (i.e., less than 10 %) would
20 react in the aqueous phase or at the surface of the droplets during cloud events, leading to the
21 formation of low volatile species, this would explain the observed amount of aqSOA formed.

22 Table 4 shows that, for triphasic experiments, the measured VOC losses in the gas phase during
23 the cloud events ($\sum \Delta C_{cloud}$) were between 1.5 and 3 times higher than the theoretical quantity
24 (Henry's Law equilibrium) transferred from the gas phase to the droplets. This result suggests
25 that: (1) a reactive uptake of VOCs toward the aqueous phase is taking place, shifting the
26 Henry's Law equilibrium and increasing the amount of VOCs transferred to the droplets, and
27 (2) a large part of this solubilized organic matter is transformed into semi-volatile species on
28 the time scale of the cloud event. This result implies a very fast reactivity in the aqueous phase,
29 which is in agreement with the observed rapid aqSOA production.

1 **3.3 SOA formation details and chemical composition**

2 For both diphasic and triphasic systems, aqSOA production reached a value of ca. $0.02 \mu\text{g m}^{-3}$
3 s^{-1} during the first 2 minutes of the cloud event (Figure S4). This value then decreased to
4 approximately $0.005 \mu\text{g m}^{-3} \text{s}^{-1}$ until cloud dissipation. Keeping the hypothesis of an
5 instantaneous Henry's Law equilibrium, the highest aqSOA production observed at the
6 beginning of the cloud event is probably due to the dissolution of the soluble species as 2
7 minutes is in the order of magnitude of the mixing time in the CESAM chamber (ca. 100 s,
8 Wang et al. (2011)) while the second (lower) production phase may be related to the shift of
9 this equilibrium due to possible reactivity in the aqueous phase.

10 In diphasic experiments, the brevity of the aqSOA formation, the small size of these aerosols
11 after cloud evaporation (a mass mode diameter of less than 100 nm) and a reduced collection
12 efficiency for particles with a <100 nm aerodynamic diameter in the HR-ToF-AMS, limit
13 quantitative results. The results for elemental ratios (O/C, H/C, and OM/OC) were hence
14 restricted to the first cloud event and around 10 minutes after, when the diameter mode of the
15 distribution was sufficiently high to achieve a reliable signal from the HR-ToF-AMS. Temporal
16 variation of elemental ratios and density for aqSOA in diphasic and triphasic systems for the
17 first cloud event are presented in Figure 3. Temporal evolutions of these elemental ratios for
18 each system were reproducible. A slight increase of O/C and OM/OC ratios was observed
19 between 5 and 10 minutes after the first cloud generation, but these variations remain
20 insignificant considering the measurement uncertainties given by Aiken et al. (2008). The
21 average values of elemental ratios in diphasic and triphasic systems (calculated using values
22 obtained during and after the first cloud event of each experiment) showed no significant
23 difference compared to the results obtained under dry conditions (Table 5). We observed no
24 change in the density which remains at $1.40 \pm 0.04 \mu\text{g m}^{-3}$ as under dry conditions (Brégonzio-
25 Rozier et al., 2015). The SOA effective density was obtained by calculation based on the
26 elemental composition of aerosol from AMS measurements (Kuwata et al., 2012)

27 To complete this SOA composition study, mass spectra and size distribution measured before,
28 during, and after cloud events in a typical triphasic experiment are presented in Figure 4.
29 Comparison of the size distributions in these various phases of the experiments shows the
30 persistence of the initial distribution of organic compounds (aerodynamic mode around 100
31 nm). When maximum aqSOA mass concentration is reached (Figure 4b), we note the presence
32 of a second mode (around 300 nm) corresponding to an aerosol composed of organics, nitrates

1 and mass fragments interpreted as ammonium. The particle sizes and compositions observed
2 for this second mode were very similar to what was observed during cloud events for diphasic
3 experiments (Figure S5). In triphasic experiments, the SOA composition, which was around
4 100% organics before cloud generation (Figure 4a), changed to a composition of organics (39
5 %), nitrates (48 %) and ammonium (13 %) during the cloud event (Figure 4b).

6 The presence of ammonium fragments is difficult to explain and it must be underlined that its
7 contribution was close to the detection limits of the AMS. In the gas phase, the corresponding
8 NH_3 contribution was far below the detection limits of the gas phase analytical techniques
9 (PTR-ToF-MS and FTIR). NH_3 contamination has been observed – and remained unexplained
10 - in a comparable simulation chamber (Bianchi et al., 2012). By contrast, the presence of nitrates
11 is in good agreement with field observations (Dall'Osto et al., 2009; Giorio et al., 2015).

12 The presence of nitrates could be due to the transfer from the gas phase to the aqueous phase of
13 nitric acid and organonitrates formed by isoprene photooxidation in the presence of NO_x (Darer
14 et al., 2011; Perring et al., 2013), although no high-resolution organonitrate peaks were
15 observed in the HR-ToF-AMS data and the NO/NO_2 mass peak ratios calculated from the
16 aerosol mass spectra, proposed to be used to ascertain the presence or absence of organonitrates
17 in HR-ToF-AMS data was the same as that of inorganic nitrate (Farmer et al., 2010). Even if
18 organonitrates were present, their hydrolysis in the aqueous phase could probably not explain
19 the presence of nitrates as Nguyen et al. (2012) showed that only less than 2% of organonitrates
20 derived from isoprene + NO_x undergo hydrolysis within up to 4h of reaction in the aqueous
21 phase.

22 After cloud evaporation, a slow decrease of the second aerosol size mode was observed (Fig.
23 4c), which can be linked to the aqSOA mass concentration decay. Photolysis of particulate
24 organonitrates was discarded as a possible explanation for this decay because controlled
25 experiments have been performed by switching the light just after cloud evaporation: they lead
26 to the same observations. Hydrolysis of organonitrates cannot be totally excluded.
27 Nevertheless, although hydrolysis lifetimes of tertiary organonitrates have been found to be in
28 the range of few minutes in diluted solutions (Darer et al., 2011; Hu et al., 2011; Rindelaub et
29 al., 2015), as already mentioned, this process is likely slow and of small importance for a
30 complex mixture of SOA organonitrates derived from isoprene + NO_x (Nguyen et al., 2012).
31 Furthermore, it is expected that these nitrates lead to polyols (Darer et al., 2011) which would
32 preferentially remain in the particulate phase due to their low vapour pressures (Compernelle
33 and Müller, 2014). If polyols formation was observed in our experiments, we would have

1 observed a loss of nitrates, but not of the associated organic fragments, which is not consistent
2 with our observations (Fig. 4b and c). As a result, it suggests that a chemical origin for the decay
3 of the second mode (which contains a large part of nitrates) is quite unlikely, and thus, that a
4 re-partitioning between particles and the walls is far more likely.

5 **4 Atmospheric implications and conclusion**

6 The impact of cloud events on an isoprene/NO_x system in the presence of light and at different
7 oxidation stages was investigated in a stainless steel simulation chamber. It was observed that
8 a single and relatively short cloud condensation cycle in the presence of irradiation led to a
9 significant aqSOA mass yield (0.002-0.004) with values between two and four times higher
10 than what was observed for isoprene photooxidation experiments carried out under dry
11 conditions (Brégonzio-Rozier et al., 2015). Even if no significant changes were noted in the
12 SOA elemental ratios, it appears that the bulk chemical aerosol composition was significantly
13 impacted by cloud events since an additional formation of particulate matter containing
14 organics, nitrate and ammonium fragments was observed. This formed aqSOA seems to be
15 metastable in the simulation chamber environment due to gas phase/wall repartitioning after
16 cloud dissipation. However, it can be assumed that in a real cloud, in the absence of walls, the
17 semi-volatile organic matter formed would remain in the aerosol/hydrometeor phase due to re-
18 condensation on pre-existing aerosol or condensation/dissolution on the remaining droplets.
19 Since clouds undergo several evapo-condensation cycles in the atmosphere, this study
20 highlights the potentially great importance of cloud chemistry on the secondary aerosol budget.
21 This study also shows the complexity of working with a multiphase system with cloud
22 generation disturbing equilibria established in dry conditions. However, as highlighted by
23 Daumit et al. (2014) and the results obtained in this study, it also shows the importance of
24 investigating that kind of systems, which is not only more realistic but also which is the only
25 way to experimentally study the competition between phase transfer, surface reaction and
26 homogeneous phase transformation.

27 Aqueous SOA formation was characterized by the appearance of a second mode which can be
28 connected with the “droplet mode” which has been previously detected in the ambient
29 atmosphere during early studies (Hering and Friedlander, 1982; John et al., 1990; Meng and
30 Seinfeld, 1994). Evidence was obtained by John et al. (1990) that this growing second mode
31 grew out of the condensation mode by the addition of water and aqueous phase oxidation

1 products. Our experiment provided here a direct simulation of the origin of a “droplet mode” in
2 the atmospheric aerosol.

3 Finally, using the elemental ratios obtained in this study (Figure 3), the aqSOA carbon mass
4 yields obtained in this study range between 0.002 to 0.004, which is an order of magnitude
5 lower than those predicted by a multiphase model performed on isoprene multiphase
6 photochemistry under comparable $\text{VOC}_{(\text{ppbC})}/\text{NO}_{\text{x}(\text{ppb})}$ ratios (Ervens et al., 2008). However, the
7 model was run using different initial conditions compared to our experiments: much lower
8 initial concentrations of isoprene and NO_x (by a factor of $\sim 10^3$ and ~ 100 respectively), pre-
9 existing wet seed particles, and lower liquid water content during cloud events were used in the
10 model. The observed difference between model and experimental results thus supports the great
11 need for the development of simulation chamber multiphase models in order to accurately
12 compare experimental results with the known multiphase photochemical processes. Overall,
13 our results emphasize the need to use the same integrated multiphase approach on other
14 chemical systems and to integrate these results in atmospheric chemistry models to improve
15 SOA formation determinations.

16

17 **Acknowledgements**

18 The authors thank Arnaud Allanic, Sylvain Ravier, Pascal Renard and Pascal Zapf for their
19 contributions in the experiments. The authors also acknowledge the institutions that have
20 provided financial support: the French National Institute for Geophysical Research (CNRS-
21 INSU) within the LEFE-CHAT program through the project “Impact de la chimie des nuages
22 sur la formation d’aérosols organiques secondaires dans l’atmosphère” and the French National
23 Agency for Research (ANR) project CUMULUS ANR-2010-BLAN-617-01. This work was
24 also supported by the EC within the I3 project “Integrating of European Simulation Chambers
25 for Investigating Atmospheric Processes” (EUROCHAMP-2, contract no. 228335). The
26 authors gratefully thank the MASSALYA instrumental platform (Aix Marseille Université,
27 ice.univ-amu.fr) for the analysis and measurements used in this paper.

28

1 References

- 2 Aiken, A. C., Decarlo, P. F., Kroll, J. H., Worsnop, D. R., Huffman, J. A., Docherty, K. S., Ulbrich, I.
3 M., Mohr, C., Kimmel, J. R., Sueper, D., Sun, Y., Zhang, Q., Trimborn, A., Northway, M., Ziemann, P.
4 J., Canagaratna, M. R., Onasch, T. B., Alfarra, M. R., Prevot, A. S. H., Dommen, J., Duplissy, J.,
5 Metzger, A., Baltensperger, U., and Jimenez, J. L.: O/C and OM/OC ratios of primary, secondary, and
6 ambient organic aerosols with high-resolution time-of-flight aerosol mass spectrometry, *Environmental
7 Science & Technology*, 42, 4478-4485, 2008.
- 8 Altieri, K. E., Seitzinger, S. P., Carlton, A. G., Turpin, B. J., Klein, G. C., and Marshall, A. G.: Oligomers
9 formed through in-cloud methylglyoxal reactions: Chemical composition, properties, and mechanisms
10 investigated by ultra-high resolution FT-ICR mass spectrometry, *Atmospheric Environment*, 42, 1476-
11 1490, 2008.
- 12 Bateman, A. P., Nizkorodov, S. A., Laskin, J., and Laskin, A.: Photolytic processing of secondary
13 organic aerosols dissolved in cloud droplets, *Physical Chemistry Chemical Physics*, 13, 12199-12212,
14 2011.
- 15 Benkelberg, H. J., Hamm, S., and Warneck, P.: Henry's law coefficients for aqueous solutions of
16 acetone, acetaldehyde and acetonitrile, and equilibrium constants for the addition compounds of acetone
17 and acetaldehyde with bisulfite, *Journal of Atmospheric Chemistry*, 20, 17-34, 1995.
- 18 Betterton, E. A. and Hoffmann, M. R.: Henry's law constants of some environmentally important
19 aldehydes, *Environmental Science & Technology*, 22, 1415-1418, 1988.
- 20 Bianchi, F., Dommen, J., Mathot, S., and Baltensperger, U.: On-line determination of ammonia at low
21 pptv mixing ratios in the CLOUD chamber, *Atmospheric Measurement Techniques*, 5, 1719-1725,
22 2012.
- 23 Brégonzio-Rozier, L., Siekmann, F., Giorio, C., Pangui, E., Morales, S. B., Temime-Roussel, B.,
24 Gratien, A., Michoud, V., Ravier, S., Cazaunau, M., Tapparo, A., Monod, A., and Doussin, J. F.:
25 Gaseous products and secondary organic aerosol formation during long term oxidation of isoprene and
26 methacrolein, *Atmos. Chem. Phys.*, 15, 2953-2968, 2015.
- 27 Canagaratna, M. R., Jayne, J. T., Jimenez, J. L., Allan, J. D., Alfarra, M. R., Zhang, Q., Onasch, T. B.,
28 Drewnick, F., Coe, H., Middlebrook, A., Delia, A., Williams, L. R., Trimborn, A. M., Northway, M. J.,
29 DeCarlo, P. F., Kolb, C. E., Davidovits, P., and Worsnop, D. R.: Chemical and microphysical
30 characterization of ambient aerosols with the aerodyne aerosol mass spectrometer, *Mass spectrometry
31 reviews*, 26, 185-222, 2007.
- 32 Carlton, A. G. and Turpin, B. J.: Particle partitioning potential of organic compounds is highest in the
33 Eastern US and driven by anthropogenic water, *Atmos. Chem. Phys.*, 13, 10203-10214, 2013.
- 34 Carlton, A. G., Turpin, B. J., Altieri, K. E., Seitzinger, S., Reff, A., Lim, H. J., and Ervens, B.:
35 Atmospheric oxalic acid and SOA production from glyoxal: Results of aqueous photooxidation
36 experiments, *Atmospheric Environment*, 41, 7588-7602, 2007.
- 37 Carlton, A. G., Turpin, B. J., Lim, H. J., Altieri, K. E., and Seitzinger, S.: Link between isoprene and
38 secondary organic aerosol (SOA): Pyruvic acid oxidation yields low volatility organic acids in clouds,
39 *Geophysical Research Letters*, 33, 2006.
- 40 Colvile, R. N., Bower, K. N., Choularton, T. W., Gallagher, M. W., Beswick, K. M., Arends, B. G., Kos,
41 G. P. A., Wobrock, W., Schell, D., Hargreaves, K. J., Storeton-West, R. L., Cape, J. N., Jones, B. M. R.,
42 Wiedensohler, A., Hansson, H. C., Wendisch, M., Acker, K., Wiprechtj, W., Pahl, S., Winkler, P.,
43 Berner, A., Krusiz, C., and Gieray, R.: Meteorology of the great dun fell cloud experiment 1993,
44 *Atmospheric Environment*, 31, 2407-2420, 1997.
- 45 Compernelle, S. and Müller, J. F.: Henry's law constants of polyols, *Atmos. Chem. Phys.*, 14, 12815-
46 12837, 2014.
- 47 Couvidat, F., Sartelet, K., and Seigneur, C.: Investigating the Impact of Aqueous-Phase Chemistry and
48 Wet Deposition on Organic Aerosol Formation Using a Molecular Surrogate Modeling Approach,
49 *Environmental Science & Technology*, 47, 914-922, 2013.

1 Dall'Osto, M., Harrison, R. M., Coe, H., and Williams, P.: Real-time secondary aerosol formation during
2 a fog event in London, *Atmos. Chem. Phys.*, 9, 2459-2469, 2009.

3 Darer, A. I., Cole-Filipiak, N. C., O'Connor, A. E., and Elrod, M. J.: Formation and Stability of
4 Atmospherically Relevant Isoprene-Derived Organosulfates and Organonitrates, *Environmental*
5 *Science & Technology*, 45, 1895-1902, 2011.

6 Daumit, K. E., Carrasquillo, A. J., Hunter, J. F., and Kroll, J. H.: Laboratory studies of the aqueous-
7 phase oxidation of polyols: submicron particles vs. bulk aqueous solution, *Atmos. Chem. Phys.*, 14,
8 10773-10784, 2014.

9 De Carlo, P. F., Kimmel, J. R., Trimborn, A., Northway, M. J., Jayne, J. T., Aiken, A. C., Gonin, M.,
10 Fuhrer, K., Horvath, T., Docherty, K. S., Worsnop, D. R., and Jimenez, J. L.: Field-Deployable, High-
11 Resolution, Time-of-Flight Aerosol Mass Spectrometer, *Analytical Chemistry*, 78, 8281-8289, 2006.

12 de Gouw, J. and Warneke, C.: Measurements of volatile organic compounds in the earth's atmosphere
13 using proton-transfer-reaction mass spectrometry, *Mass spectrometry reviews*, 26, 223-257, 2007.

14 de Gouw, J., Warneke, C., Karl, T., Eerdekens, G., van der Veen, C., and Fall, R.: Sensitivity and
15 specificity of atmospheric trace gas detection by proton-transfer-reaction mass spectrometry,
16 *International Journal of Mass Spectrometry*, 223-224, 365-382, 2003a.

17 de Gouw, J. A., Goldan, P. D., Warneke, C., Kuster, W. C., Roberts, J. M., Marchewka, M., Bertman,
18 S. B., Pszenny, A. A. P., and Keene, W. C.: Validation of proton transfer reaction-mass spectrometry
19 (PTR-MS) measurements of gas-phase organic compounds in the atmosphere during the New England
20 Air Quality Study (NEAQS) in 2002, *Journal of Geophysical Research: Atmospheres*, 108, n/a-n/a,
21 2003b.

22 Dommen, J., Metzger, A., Duplissy, J., Kalberer, M., Alfarra, M. R., Gascho, A., Weingartner, E.,
23 Prevot, A. S. H., Verheggen, B., and Baltensperger, U.: Laboratory observation of oligomers in the
24 aerosol from isoprene/NO_x photooxidation, *Geophysical Research Letters*, 33, L13805, 2006.

25 Dunlea, E. J., Herndon, S. C., Nelson, D. D., Volkamer, R. M., San Martini, F., Sheehy, P. M., Zahniser,
26 M. S., Shorter, J. H., Wormhoudt, J. C., Lamb, B. K., Allwine, E. J., Gaffney, J. S., Marley, N. A.,
27 Grutter, M., Marquez, C., Blanco, S., Cardenas, B., Retama, A., Ramos Villegas, C. R., Kolb, C. E.,
28 Molina, L. T., and Molina, M. J.: Evaluation of nitrogen dioxide chemiluminescence monitors in a
29 polluted urban environment, *Atmospheric Chemistry and Physics*, 7, 2691-2704, 2007.

30 Edney, E. O., Kleindienst, T. E., Jaoui, M., Lewandowski, M., Offenberg, J. H., Wang, W., and Claeys,
31 M.: Formation of 2-methyl tetrols and 2-methylglyceric acid in secondary organic aerosol from
32 laboratory irradiated isoprene/NO_x/SO₂/air mixtures and their detection in ambient PM_{2.5} samples
33 collected in the eastern United States, *Atmospheric Environment*, 39, 5281-5289, 2005.

34 El Haddad, I., Liu, Y., Nieto-Gligorovski, L., Michaud, V., Temime-Roussel, B., Quivet, E., Marchand,
35 N., Sellegri, K., and Monod, A.: In-cloud processes of methacrolein under simulated conditions - Part
36 2: Formation of secondary organic aerosol, *Atmospheric Chemistry and Physics*, 9, 5107-5117, 2009.

37 Ellis, A. M. and Mayhew, C. A.: *Proton Transfer Reaction Mass Spectrometry Principles and*
38 *Applications*, John Wiley & Sons Ltd, Chichester, United Kingdom, 2014.

39 Ervens, B., Carlton, A. G., Turpin, B. J., Altieri, K. E., Kreidenweis, S. M., and Feingold, G.: Secondary
40 organic aerosol yields from cloud-processing of isoprene oxidation products, *Geophysical Research*
41 *Letters*, 35, 2008.

42 Ervens, B., Sorooshian, A., Lim, Y. B., and Turpin, B. J.: Key parameters controlling OH-initiated
43 formation of secondary organic aerosol in the aqueous phase (aqSOA), *Journal of Geophysical*
44 *Research-Atmospheres*, 119, 3997-4016, 2014.

45 Ervens, B., Turpin, B. J., and Weber, R. J.: Secondary organic aerosol formation in cloud droplets and
46 aqueous particles (aqSOA): a review of laboratory, field and model studies, *Atmospheric Chemistry and*
47 *Physics*, 11, 11069-11102, 2011.

48 Farmer, D. K., Matsunaga, A., Docherty, K. S., Surratt, J. D., Seinfeld, J. H., Ziemann, P. J., and
49 Jimenez, J. L.: Response of an aerosol mass spectrometer to organonitrates and organosulfates and

1 implications for atmospheric chemistry, Proceedings of the National Academy of Sciences of the United
2 States of America, 107, 6670-6675, 2010.

3 Galloway, M. M., Huisman, A. J., Yee, L. D., Chan, A. W. H., Loza, C. L., Seinfeld, J. H., and Keutsch,
4 F. N.: Yields of oxidized volatile organic compounds during the OH radical initiated oxidation of
5 isoprene, methyl vinyl ketone, and methacrolein under high-NO_x conditions, Atmospheric Chemistry
6 and Physics, 11, 10779-10790, 2011.

7 Giorio, C., Tapparo, A., Dall'Osto, M., Beddows, D. C. S., Esser-Gietl, J. K., Healy, R. M., and
8 Harrison, R. M.: Local and Regional Components of Aerosol in a Heavily Trafficked Street Canyon in
9 Central London Derived from PMF and Cluster Analysis of Single-Particle ATOFMS Spectra,
10 Environmental Science & Technology, 49, 3330-3340, 2015.

11 Hallquist, M., Wenger, J. C., Baltensperger, U., Rudich, Y., Simpson, D., Claeys, M., Dommen, J.,
12 Donahue, N. M., George, C., Goldstein, A. H., Hamilton, J. F., Herrmann, H., Hoffmann, T., Iinuma,
13 Y., Jang, M., Jenkin, M. E., Jimenez, J. L., Kiendler-Scharr, A., Maenhaut, W., McFiggans, G., Mentel,
14 T. F., Monod, A., Prevot, A. S. H., Seinfeld, J. H., Surratt, J. D., Szmigielski, R., and Wildt, J.: The
15 formation, properties and impact of secondary organic aerosol: current and emerging issues,
16 Atmospheric Chemistry and Physics, 9, 5155-5236, 2009.

17 Herckes, P., Valsaraj, K. T., and Collett Jr, J. L.: A review of observations of organic matter in fogs and
18 clouds: Origin, processing and fate, Atmospheric Research, doi:
19 <http://dx.doi.org/10.1016/j.atmosres.2013.06.005>, 2013. 2013.

20 Hering, S. V. and Friedlander, S. K.: Origins of aerosol sulfur size distributions in the Los Angeles
21 basin, Atmospheric Environment (1967), 16, 2647-2656, 1982.

22 Herrmann, H.: Kinetics of Aqueous Phase Reactions Relevant for Atmospheric Chemistry, Chemical
23 Reviews, 103, 4691-4716, 2003.

24 Herrmann, H., Schaefer, T., Tilgner, A., Styler, S. A., Weller, C., Teich, M., and Otto, T.: Tropospheric
25 Aqueous-Phase Chemistry: Kinetics, Mechanisms, and Its Coupling to a Changing Gas Phase, Chemical
26 Reviews, 115, 4259-4334, 2015.

27 Hilal, S. H., Ayyampalayam, S. N., and Carreira, L. A.: Air-Liquid Partition Coefficient for a Diverse
28 Set of Organic Compounds: Henry's Law Constant in Water and Hexadecane, Environmental Science
29 & Technology, 42, 9231-9236, 2008.

30 Hu, K. S., Darer, A. I., and Elrod, M. J.: Thermodynamics and kinetics of the hydrolysis of
31 atmospherically relevant organonitrates and organosulfates, Atmos. Chem. Phys., 11, 8307-8320, 2011.

32 Huang, X.-F., Yu, J. Z., He, L.-Y., and Yuan, Z.: Water-soluble organic carbon and oxalate in aerosols
33 at a coastal urban site in China: Size distribution characteristics, sources, and formation mechanisms,
34 Journal of Geophysical Research: Atmospheres, 111, D22212, 2006.

35 IPCC: : Climate Change 2013: The Physical Science Basis. Contribution of Working Group I to the
36 Fifth Assessment Report of the Intergovernmental Panel on Climate Change, [Stocker, T.F., D. Qin, G.-
37 K. Plattner, M. Tignor, S.K. Allen, J. Boschung, A. Nauels, Y. Xia, V. Bex and P.M. Midgley (eds.)],
38 Cambridge, United Kingdom and New York, NY, USA, 2013.

39 John, W., Wall, S. M., Ondo, J. L., and Winklmayr, W.: Modes in the size distributions of atmospheric
40 inorganic aerosol, Atmospheric Environment. Part A. General Topics, 24, 2349-2359, 1990.

41 Kanakidou, M., Seinfeld, J. H., Pandis, S. N., Barnes, I., Dentener, F. J., Facchini, M. C., Van Dingenen,
42 R., Ervens, B., Nenes, A., Nielsen, C. J., Swietlicki, E., Putaud, J. P., Balkanski, Y., Fuzzi, S., Horth, J.,
43 Moortgat, G. K., Winterhalter, R., Myhre, C. E. L., Tsigaridis, K., Vignati, E., Stephanou, E. G., and
44 Wilson, J.: Organic aerosol and global climate modelling: a review, Atmospheric Chemistry and
45 Physics, 5, 1053-1123, 2005.

46 Kleindienst, T. E., Edney, E. O., Lewandowski, M., Offenbergl, J. H., and Jaoui, M.: Secondary organic
47 carbon and aerosol yields from the irradiations of isoprene and alpha-pinene in the presence of NO_x and
48 SO₂, Environmental Science & Technology, 40, 3807-3812, 2006.

1 Kroll, J. H., Ng, N. L., Murphy, S. M., Flagan, R. C., and Seinfeld, J. H.: Secondary organic aerosol
2 formation from isoprene photooxidation under high-NO_x conditions, *Geophysical Research Letters*, 32,
3 2005.

4 Kuwata, M., Zorn, S. R., and Martin, S. T.: Using Elemental Ratios to Predict the Density of Organic
5 Material Composed of Carbon, Hydrogen, and Oxygen, *Environmental Science & Technology*, 46, 787-
6 794, 2012.

7 Lee, A. K. Y., Hayden, K. L., Herckes, P., Leaitch, W. R., Liggio, J., Macdonald, A. M., and Abbatt, J.
8 P. D.: Characterization of aerosol and cloud water at a mountain site during WACS 2010: secondary
9 organic aerosol formation through oxidative cloud processing, *Atmos. Chem. Phys.*, 12, 7103-7116,
10 2012.

11 Leng, C., Kish, J. D., Kelley, J., Mach, M., Hiltner, J., Zhang, Y., and Liu, Y.: Temperature-Dependent
12 Henry's Law Constants of Atmospheric Organics of Biogenic Origin, *The Journal of Physical Chemistry*
13 *A*, 117, 10359-10367, 2013.

14 Lim, Y. B., Tan, Y., and Turpin, B. J.: Chemical insights, explicit chemistry, and yields of secondary
15 organic aerosol from OH radical oxidation of methylglyoxal and glyoxal in the aqueous phase,
16 *Atmospheric Chemistry and Physics*, 13, 8651-8667, 2013.

17 Lin, P., Huang, X.-F., He, L.-Y., and Yu, J. Z.: Abundance and size distribution of HULIS in ambient
18 aerosols at a rural site in South China, *Journal of Aerosol Science*, 41, 74-87, 2010.

19 Liu, Y., Monod, A., Tritscher, T., Praplan, A. P., DeCarlo, P. F., Temime-Roussel, B., Quivet, E.,
20 Marchand, N., Dommen, J., and Baltensperger, U.: Aqueous phase processing of secondary organic
21 aerosol from isoprene photooxidation, *Atmos. Chem. Phys.*, 12, 5879-5895, 2012a.

22 Liu, Y., Siekmann, F., Renard, P., El Zein, A., Salque, G., El Haddad, I., Temime-Roussel, B., Voisin,
23 D., Thissen, R., and Monod, A.: Oligomer and SOA formation through aqueous phase photooxidation
24 of methacrolein and methyl vinyl ketone, *Atmospheric Environment*, 49, 123-129, 2012b.

25 Loza, C. L., Chan, A. W. H., Galloway, M. M., Keutsch, F. N., Flagan, R. C., and Seinfeld, J. H.:
26 Characterization of Vapor Wall Loss in Laboratory Chambers, *Environmental Science & Technology*,
27 44, 5074-5078, 2010.

28 Matsunaga, A. and Ziemann, P. J.: Gas-Wall Partitioning of Organic Compounds in a Teflon Film
29 Chamber and Potential Effects on Reaction Product and Aerosol Yield Measurements, *Aerosol Science*
30 *and Technology*, 44, 881-892, 2010.

31 Meng, Z. and Seinfeld, J. H.: On the Source of the Submicrometer Droplet Mode of Urban and Regional
32 Aerosols, *Aerosol Science and Technology*, 20, 253-265, 1994.

33 Michoud, V., Colomb, A., Borbon, A., Miet, K., Beekmann, M., Camredon, M., Aumont, B., Perrier,
34 S., Zapf, P., Siour, G., Ait-Helal, W., Afif, C., Kukui, A., Furger, M., Dupont, J. C., Haefelin, M., and
35 Doussin, J. F.: Study of the unknown HONO daytime source at a European suburban site during the
36 MEGAPOLI summer and winter field campaigns, *Atmos. Chem. Phys.*, 14, 2805-2822, 2014.

37 Middlebrook, A. M., Bahreini, R., Jimenez, J. L., and Canagaratna, M. R.: Evaluation of Composition-
38 Dependent Collection Efficiencies for the Aerodyne Aerosol Mass Spectrometer using Field Data,
39 *Aerosol Science and Technology*, 46, 258-271, 2012.

40 Nguyen, T. B., Laskin, A., Laskin, J., and Nizkorodov, S. A.: Direct aqueous photochemistry of isoprene
41 high-NO_x secondary organic aerosol, *Physical Chemistry Chemical Physics*, 14, 9702-9714, 2012.

42 Ortiz-Montalvo, D. L., Lim, Y. B., Perri, M. J., Seitzinger, S. P., and Turpin, B. J.: Volatility and Yield
43 of Glycolaldehyde SOA Formed through Aqueous Photochemistry and Droplet Evaporation, *Aerosol*
44 *Science and Technology*, 46, 1002-1014, 2012.

45 Peltier, R. E., Hecobian, A. H., Weber, R. J., Stohl, A., Atlas, E. L., Riemer, D. D., Blake, D. R., Apel,
46 E., Campos, T., and Karl, T.: Investigating the sources and atmospheric processing of fine particles from
47 Asia and the Northwestern United States measured during INTEX B, *Atmospheric Chemistry and*
48 *Physics*, 8, 1835-1853, 2008.

1 Perri, M. J., Seitzinger, S., and Turpin, B. J.: Secondary organic aerosol production from aqueous
2 photooxidation of glycolaldehyde: Laboratory experiments, *Atmospheric Environment*, 43, 1487-1497,
3 2009.

4 Perring, A. E., Pusede, S. E., and Cohen, R. C.: An Observational Perspective on the Atmospheric
5 Impacts of Alkyl and Multifunctional Nitrates on Ozone and Secondary Organic Aerosol, *Chemical*
6 *Reviews*, 113, 5848-5870, 2013.

7 Poulain, L., Katrib, Y., Isikli, E., Liu, Y., Wortham, H., Mirabel, P., Le Calve, S., and Monod, A.: In-
8 cloud multiphase behaviour of acetone in the troposphere: Gas uptake, Henry's law equilibrium and
9 aqueous phase photooxidation, *Chemosphere*, 81, 312-320, 2010.

10 Raventos-Duran, T., Camredon, M., Valorso, R., Mouchel-Vallon, C., and Aumont, B.: Structure-
11 activity relationships to estimate the effective Henry's law constants of organics of atmospheric interest,
12 *Atmospheric Chemistry and Physics*, 10, 7643-7654, 2010.

13 Reed Harris, A. E., Ervens, B., Shoemaker, R. K., Kroll, J. A., Rapf, R. J., Griffith, E. C., Monod, A.,
14 and Vaida, V.: Photochemical Kinetics of Pyruvic Acid in Aqueous Solution, *The Journal of Physical*
15 *Chemistry A*, 118, 8505-8516, 2014.

16 Rindelaub, J. D., McAvey, K. M., and Shepson, P. B.: The photochemical production of organic nitrates
17 from α -pinene and loss via acid-dependent particle phase hydrolysis, *Atmospheric Environment*, 100,
18 193-201, 2015.

19 Schwartz, S. E.: Mass-transport considerations pertinent to aqueous-phase reactions of gases in liquid-
20 water clouds, *Chemistry of Multiphase Atmospheric Systems*, NATO ASI Series, Vol. G6, 1986.

21 Staudinger, J. and Roberts, P. V.: A critical compilation of Henry's law constant temperature dependence
22 relations for organic compounds in dilute aqueous solutions, *Chemosphere*, 44, 561-576, 2001.

23 Staudinger, J. and Roberts, P. V.: A critical review of Henry's law constants for environmental
24 applications, *Critical Reviews in Environmental Science and Technology*, 26, 205-297, 1996.

25 Stubenrauch, C. J., Rossow, W. B., Kinne, S., Ackerman, S., Cesana, G., Chepfer, H., Di Girolamo, L.,
26 Getzewich, B., Guignard, A., Heidinger, A., Maddux, B. C., Menzel, W. P., Minnis, P., Pearl, C.,
27 Platnick, S., Poulsen, C., Riedi, J., Sun-Mack, S., Walther, A., Winker, D., Zeng, S., and Zhao, G.:
28 Assessment of Global Cloud Datasets from Satellites: Project and Database Initiated by the GEWEX
29 Radiation Panel, *Bulletin of the American Meteorological Society*, 94, 1031-1049, 2013.

30 Tan, Y., Lim, Y. B., Altieri, K. E., Seitzinger, S. P., and Turpin, B. J.: Mechanisms leading to oligomers
31 and SOA through aqueous photooxidation: insights from OH radical oxidation of acetic acid and
32 methylglyoxal, *Atmos. Chem. Phys.*, 12, 801-813, 2012.

33 Wang, J., Doussin, J. F., Perrier, S., Perraudin, E., Katrib, Y., Pangu, E., and Picquet-Varrault, B.:
34 Design of a new multi-phase experimental simulation chamber for atmospheric photosmog, aerosol and
35 cloud chemistry research, *Atmospheric Measurement Techniques*, 4, 2465-2494, 2011.

36 Warneke, C., Veres, P., Holloway, J. S., Stutz, J., Tsai, C., Alvarez, S., Rappenglueck, B., Fehsenfeld,
37 F. C., Graus, M., Gilman, J. B., and de Gouw, J. A.: Airborne formaldehyde measurements using PTR-
38 MS: calibration, humidity dependence, inter-comparison and initial results, *Atmospheric Measurement*
39 *Techniques*, 4, 2345-2358, 2011.

40 Wylie, D., Jackson, D. L., Menzel, W. P., and Bates, J. J.: Trends in Global Cloud Cover in Two Decades
41 of HIRS Observations, *Journal of Climate*, 18, 3021-3031, 2005.

42 Zhang, H., Surratt, J. D., Lin, Y. H., Bapat, J., and Kamens, R. M.: Effect of relative humidity on SOA
43 formation from isoprene/NO photooxidation: enhancement of 2-methylglyceric acid and its
44 corresponding oligoesters under dry conditions, *Atmospheric Chemistry and Physics*, 11, 6411-6424,
45 2011.

46 Zhang, Q., Jimenez, J. L., Canagaratna, M. R., Allan, J. D., Coe, H., Ulbrich, I., Alfarra, M. R., Takami,
47 A., Middlebrook, A. M., Sun, Y. L., Dzepina, K., Dunlea, E., Docherty, K., DeCarlo, P. F., Salcedo, D.,
48 Onasch, T., Jayne, J. T., Miyoshi, T., Shimojo, A., Hatakeyama, S., Takegawa, N., Kondo, Y.,
49 Schneider, J., Drewnick, F., Borrmann, S., Weimer, S., Demerjian, K., Williams, P., Bower, K.,
50 Bahreini, R., Cottrell, L., Griffin, R. J., Rautiainen, J., Sun, J. Y., Zhang, Y. M., and Worsnop, D. R.:

1 Ubiquity and dominance of oxygenated species in organic aerosols in anthropogenically-influenced
2 Northern Hemisphere midlatitudes, *Geophysical Research Letters*, 34, L13801, 2007.

3 Zhang, X., Cappa, C. D., Jathar, S. H., McVay, R. C., Ensberg, J. J., Kleeman, M. J., and Seinfeld, J.
4 H.: Influence of vapor wall loss in laboratory chambers on yields of secondary organic aerosol,
5 *Proceedings of the National Academy of Sciences of the United States of America*, 111, 5802-5807,
6 2014.

7 Zhou, X., Huang, G., Civerolo, K., and Schwab, J.: Measurement of Atmospheric Hydroxyacetone,
8 Glycolaldehyde, and Formaldehyde, *Environmental Science & Technology*, 43, 2753-2759, 2009.

9 Zhou, X. L., Qiao, H. C., Deng, G. H., and Civerolo, K.: A method for the measurement of atmospheric
10 HONO based on DNPH derivatization and HPLC analysis, *Environmental Science & Technology*, 33,
11 3672-3679, 1999.

12
13
14

1 Table 1: Comparisons of cloud properties between clouds generated in CESAM (23 clouds)
 2 and atmospheric clouds (Colvile et al., 1997; Herrmann, 2003).

| | CESAM | Atmosphere |
|---|---|----------------------------------|
| Droplet lifetime (min) | 6-13* | ≈2-30 |
| Liquid Water Content (g m⁻³) | Maximum: 0.01-1.48 Average : 0.005-0.62 | 0.05-3 |
| Mean mass-weighed diameter (μm) | 3.5-8 | 1-25 |
| Number concentration (droplet cm⁻³) | Maximum: 1×10 ³ -5×10 ⁴ Average : 4×10 ² -1×10 ⁴ | 10 ² -10 ³ |
| Mean number-weighed diameter (μm) | 2-4 | 1-25 |

3 *Droplets lifetimes correspond to clouds lifetimes.

4

1 Table 2: Initial experimental conditions, maximum aerosol mass obtained under dry conditions
 2 and information on the generated clouds.

| Experiment ^{a,b} | [Isoprene] _i (ppb) | [NO] _i (ppb) | [NO ₂] _i ^c (ppb) | [HONO] _i (ppb) | ΔM ₀ ^d (μg m ⁻³) | T _i (°C) | Number of clouds | LWC _{max} ^e (g m ⁻³) |
|------------------------------|----------------------------------|----------------------------|---|------------------------------|---|------------------------|---------------------|---|
| Diphasic experiments | | | | | | | | |
| D300113 | 817 | 95 | 71 | 161 | / | 21 | 2 | 0.87 0.45 |
| D010213 | 800 | 103 | 49 | 133 | / | 21.1 | 2 | 1.41 0.74 |
| D190313 | 831 | 123 | 58 | 99 | / | 19.8 | 3 | 0.49 0.77 0.57 |
| Triphasic experiments | | | | | | | | |
| T160113 | 846 | 143 | 27 | 15 | < 0.1 | 21.5 | 1 | 0.47 |
| T280113 | 833 | 88 | 45 | 125 | 2.8 | 18.3 | 2 | 0.81 0.88 |
| T130313 | 840 | 66 | < 1 | 45 | 2.4 | 17.5 | 1 | n.m. ^f |
| T250313 | 802 | 137 | 48 | 121 | 0.15 | 19.7 | 2 | 0.02 0.01 |

3 ^aAll experiments were carried out at initial RH < 5 %.

4 ^bExperimental IDs starting with “D” indicate diphasic experiments and experimental IDs
 5 starting with “T” indicate triphasic experiments.

6 ^cCorrected for HONO interference.

7 ^dgasSOA mass concentration using an effective density of 1.4 g cm⁻³ (Brégonzio-Rozier et al.,
 8 2015). There is no initial gasSOA formation for diphasic experiments.

9 ^eLWC_{max} of each cloud generated.

10 ^f not measured.

11

12

13

1 Table 3: Summary of the maxima increases of the total particle mass concentration observed
 2 during cloud events for diphasic and triphasic experiments.

| Experiment* | Increase in mass ($\mu\text{g m}^{-3}$) | Cloud lifetime (min) |
|-------------------------------------|---|---------------------------------|
| Diphasic experiments | | |
| D300113 1st cloud | 8.0 | 12 |
| D300113 2nd cloud | 5.1 | 9 |
| D010213 1st cloud | 6.1 | 13 |
| D010213 2nd cloud | 1.9 | 9 |
| D190313 1st cloud | 3.9 | 11 |
| D190313 2nd cloud | 2.6 | 12 |
| D190313 3rd cloud | 2.7 | 11 |
| Triphasic experiments | | |
| T160113 | 6.4 | 10 |
| T280113 1st cloud | 6.5 | 10 |
| T280113 2nd cloud | 5.5 | 10 |
| T130313 | 7.2 | 11 |
| T250313 1st cloud | 4.3 | 9 |
| T250313 2nd cloud | 2.1 | 6 |

3 *Experimental IDs starting with “D” indicate diphasic experiments, experimental IDs starting
 4 with “T” indicate triphasic experiments.

5

6

1 Table 4: Comparison between measured VOC loss, potential aqueous phase dissolution of gas
 2 phase species and particle formation during cloud events of each system.

| | Diphasic system | | Triphasic system | | K_H^* (M atm ⁻¹) | Reference |
|--|---|-------------|------------------|--------------|-----------------------------------|---|
| | D300113 | D010213 | T160113 | T280113 | | |
| | ΔC_{cloud}^a ($\mu\text{g m}^{-3}$) and relative change (%) | | | | | |
| Isoprene ^g | 0 | 0 | 0 | 0 | 3.4×10^{-2} | Leng et al. (2013) |
| C ₄ H ₆ O ^g : | 0 | 0 | 0 | 0 | | |
| MACR | | | | | 9.5 | Hilal et al. (2008) |
| MVK | | | | | 18 | Hilal et al. (2008) |
| Acrolein | 1.1 (19 %) | 0.9 (16 %) | 2.7 (41 %) | 2.3 (30 %) | 9.5 | Hilal et al. (2008) |
| 3-methylfuran | 1.7 (15 %) | 1.7 (14 %) | 0 | 0 | 6.1^d | Hilal et al. (2008) |
| Acetaldehyde | 1.3 (3 %) | 0.7 (2 %) | 4.3 (9 %) | 5.6 (11 %) | 13 | Benkelberg et al. (1995) |
| Acetone ^g | 0 | 0 | 0 | 0 | 33 | Poulain et al. (2010) |
| Formaldehyde | - | - | - | - | 3.2×10^3 | Staudinger and Roberts (1996) |
| Methylglyoxal | 34.4 (49 %) | 32.1 (49 %) | 23 (52 %) | 31.2 (42 %) | 3.7×10^3 | Betterton and Hoffmann (1988) |
| C ₂ H ₄ O ₂ : | 59.4 (37 %) | 58.4 (36 %) | 141.4 (46 %) | 143.2 (35 %) | | |
| Acetic acid ^b | | | | | 4.6×10^3 | Staudinger and Roberts (2001) |
| Glycolaldehyde | | | | | 4.1×10^4 | Betterton and Hoffmann (1988) |
| Formic acid ^b | 49.1 (41 %) | 47.8 (38 %) | 107.8 (49 %) | 177.2 (48 %) | 6.7×10^3 | Staudinger and Roberts (2001) |
| Hydroxyacetone | 15.4 (32 %) | 18.2 (37 %) | 32.1(47 %) | 26.3 (36 %) | 7.8×10^3 | Zhou et al. (2009) |
| C ₄ H ₆ O ₂ : | 1.4 (7 %) | 2.2 (11 %) | 3.6 (26 %) | 3.2 (18 %) | | |
| 3-oxobutanal ^c | | | | | 1.1×10^4 | Estimated using GROMHE (Raventos-Duran et al., 2010) |
| hydroxyMVK ^c | | | | | 1.9×10^3 | |
| C ₅ H ₈ O ^g : | 0 | 0 | 0 | 0 | 27.1 | Estimated using GROMHE (Raventos-Duran et al., 2010) |
| 2-methylbut-3-enal ^c | | | | | | |
| C ₅ H ₆ O ₂ : | 7.6 (41 %) | 8 (39 %) | 17.6 (55 %) | 3.2 (36 %) | 2.0×10^4 | Estimated using GROMHE (Raventos-Duran et al., 2010) |
| 2-methyl-but-2-enedial ^c | | | | | | |
| C ₅ H ₄ O ₃ ^c | 4.6 (43 %) | 5 (46 %) | 8.2 (69 %) | 3.2 (54 %) | $\gg 10^4$ | - |
| Measured VOCs loss after cloud evaporation^e ($\mu\text{g m}^{-3}$) | 176 | 175 | 341 | 395 | | |
| Expected VOCs dissolution in water at cloud start^f ($\mu\text{g m}^{-3}$) | 136 | 198 | 121 | 272 | | |
| Maximum particle mass concentration enhancement measured during cloud event ($\mu\text{g m}^{-3}$) | 8.0 | 6.1 | 6.4 | 6.5 | | |
| LWC_{max} first cloud (g m⁻³) | 0.87 | 1.41 | 0.47 | 0.81 | | |

3 ^a $\Delta C_{cloud} = C_{before} - C_{after}$. C_{after} corresponds to mixing ratios measured 20 minutes after cloud
 4 evaporation, when the PTR-ToF-MS signal was stabilized for all compounds.

1 ^bThe acids were considered undissociated.

2 ^cC₄H₆O₂ was attributed to 3-oxobutanal and hydroxyMVK ; C₅H₈O and C₅H₆O₂ were attributed
3 to 2-methylbut-3-enal and 2-methyl-but-2-enedial respectively, and C₅H₄O₃ could not be
4 attributed to any known isoprene product (Brégonzio-Rozier et al., 2015).

5 ^dEffective Henry's Law constant of 3-methylfuran was assumed identical to the one of 2-
6 methyltetrahydrofuran.

7 ^eTotal VOC loss ($\sum \Delta C_{cloud}$) as measured by the PTR-ToF-MS (excluding formaldehyde for
8 which the strong humidity-dependent sensitivity was not assessed) 20 minutes after cloud
9 evaporation.

10 ^fDissolution of VOCs is calculated assuming Henry's Law equilibrium at cloud start (see
11 Supplement Sect. 1). Formaldehyde cannot be accurately quantified by PTR-MS under highly
12 variable humidity conditions (Warneke et al., 2011). As a result, formaldehyde mixing ratios
13 used for calculations were taken at low relative humidity, before water vapour injection.

14 ^gThese species were excluded from VOCs loss calculation as their decay from gas phase
15 chemistry did not sound affected by the cloud events.

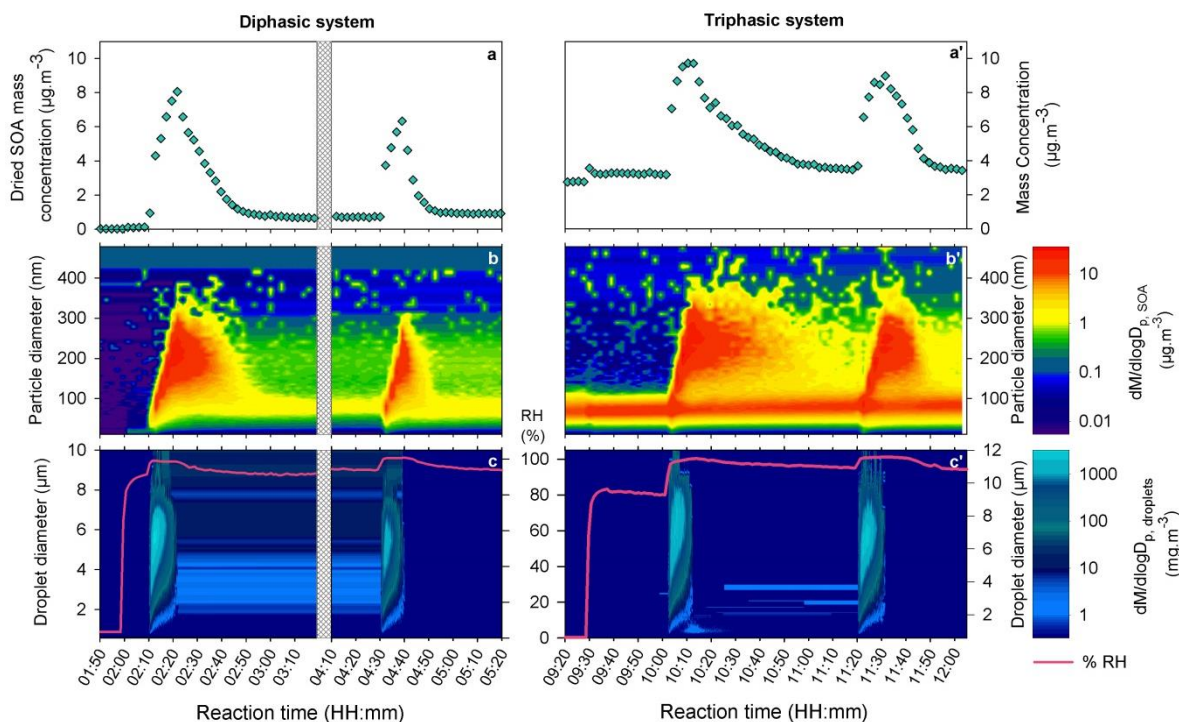
16

1 Table 5 Average elemental ratios of SOA from isoprene photooxidation under dry conditions
2 and after cloud generation (diphasic and triphasic experiments). Values in parentheses reflect
3 the measurement uncertainty as determined by Aiken et al. (2008).

| O/C | OM/OC | H/C | Reference |
|---------------------|---------------------|---------------------|---|
| 0.58 (± 0.18) | 1.90 (± 0.11) | 1.45 (± 0.15) | Diphasic experiments |
| 0.58 (± 0.18) | 1.89 (± 0.11) | 1.39 (± 0.14) | Triphasic experiments |
| 0.60 (± 0.19) | 1.92 (± 0.12) | 1.43 (± 0.14) | Dry conditions (Brégonzio-Rozier et al., 2015) |

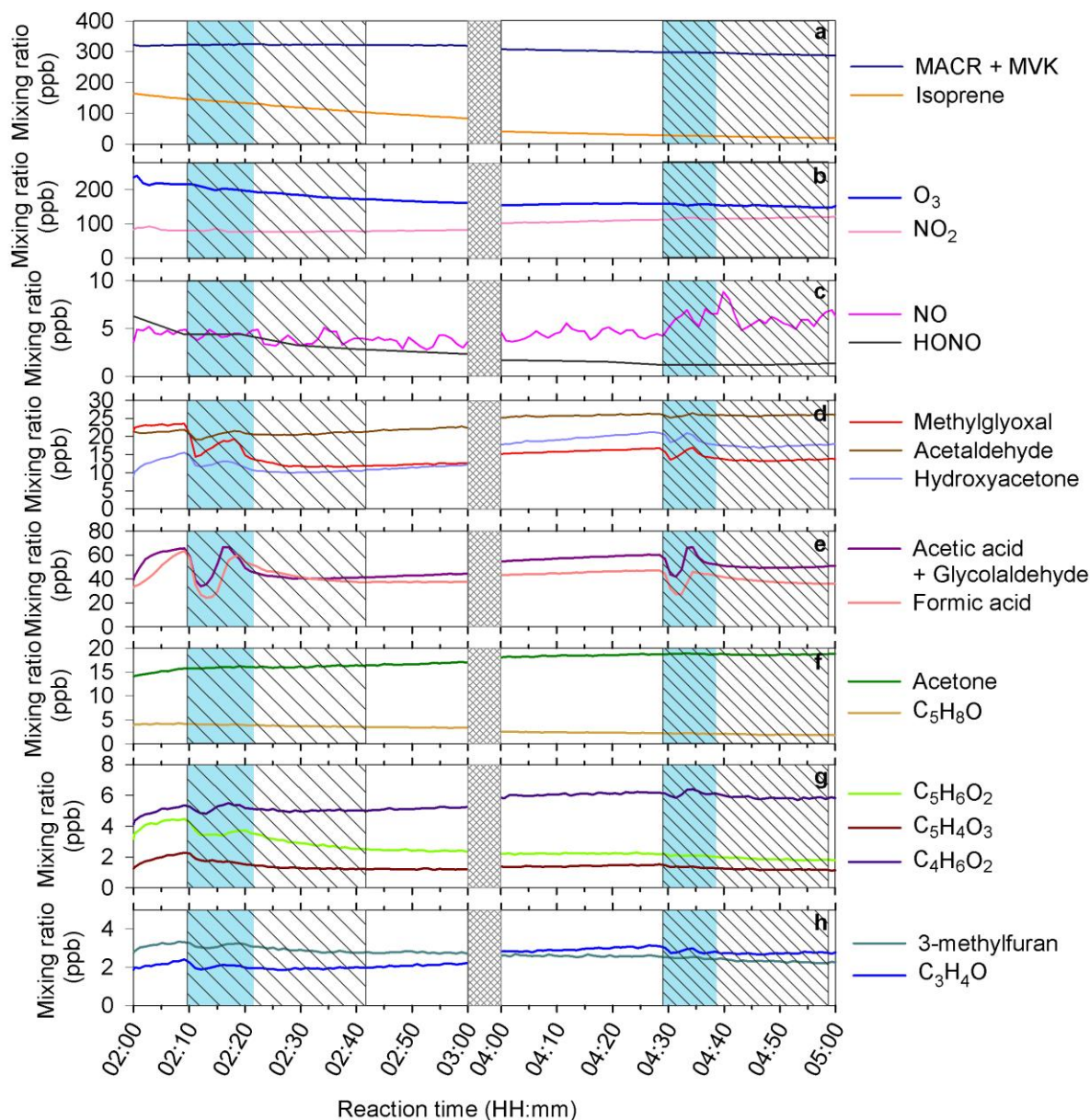
4

5



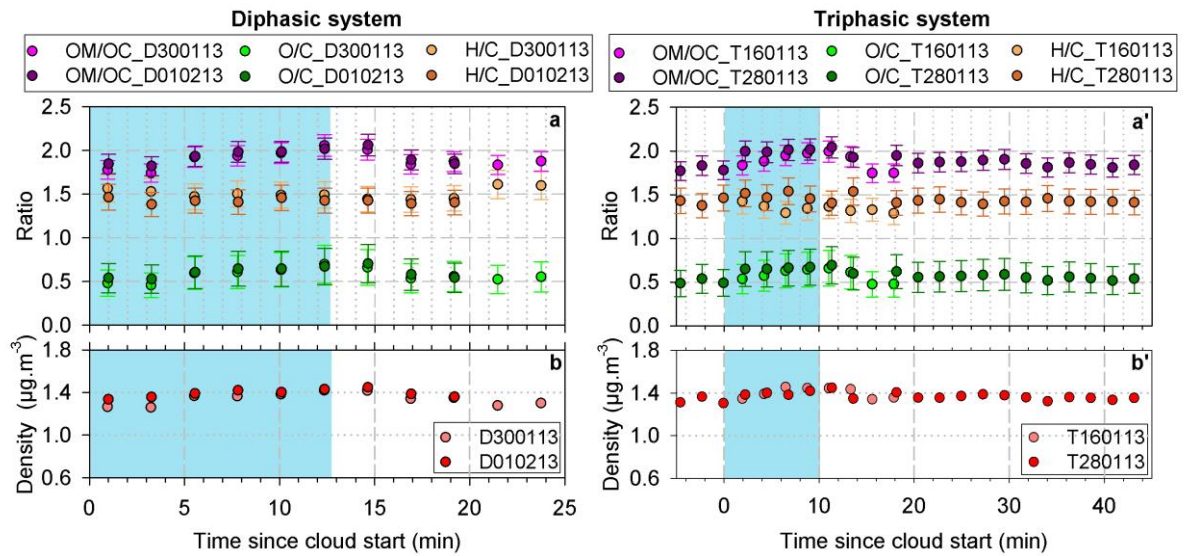
1
 2 Figure 1: Effects of liquid phase clouds on SOA mass concentrations during two cloud events
 3 for typical diphasic (D300113, left panel) and triphasic (T280113, right panel) systems. Time
 4 profiles of (a and a') dried SOA mass concentration, (b and b') dried SOA mass size
 5 distribution, (c and c') cloud droplets mass size distribution and relative humidity in the
 6 simulation chamber. A particle density of $1.4 \mu\text{g m}^{-3}$ was assumed.

7



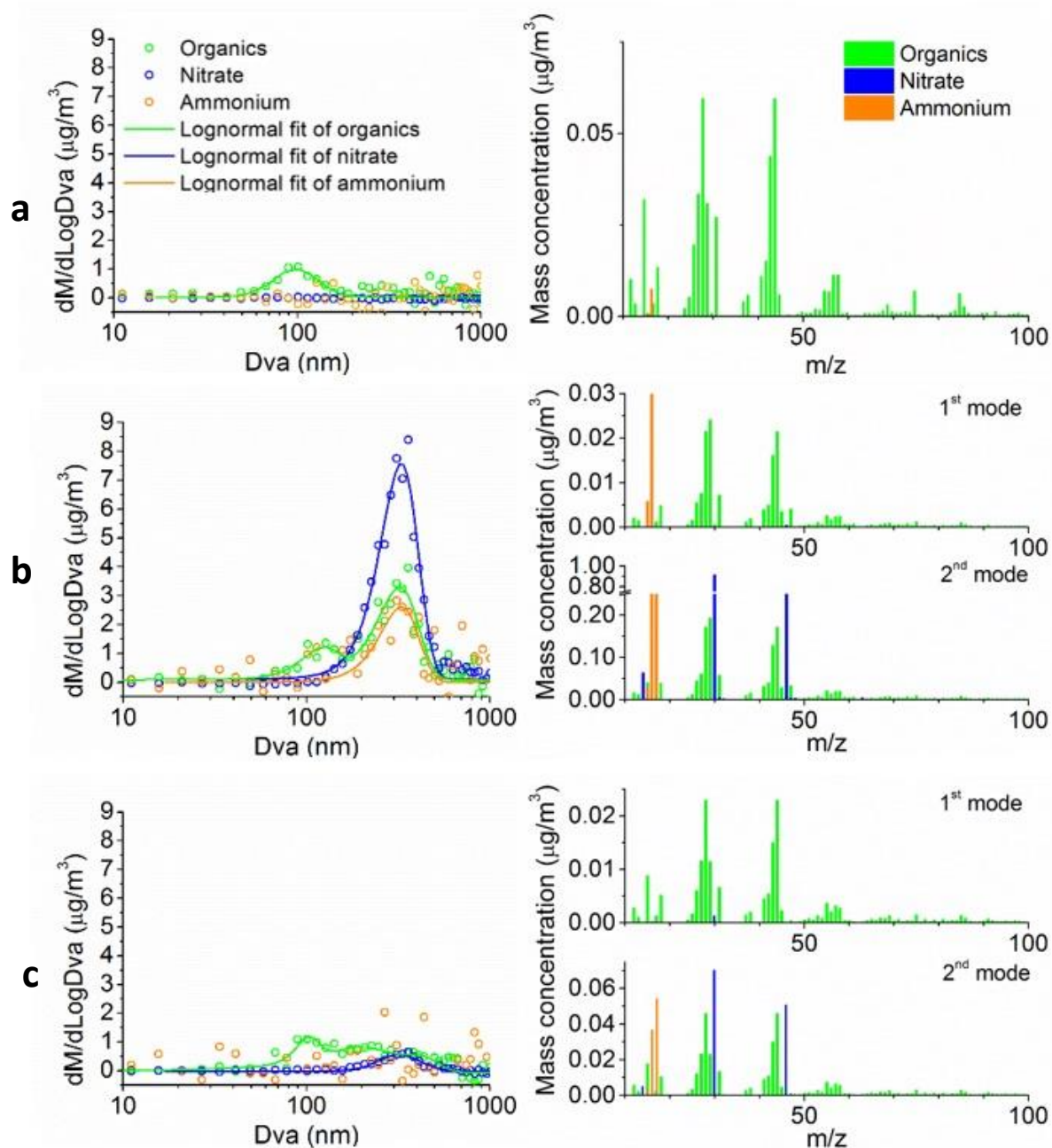
1
 2 Figure 2: Time profiles of the gas phase reactants and isoprene oxidation products during a
 3 diphasic experiment (D300113). Blue areas indicate cloud events and hatched area indicate time
 4 needed for the PTR-ToF-MS signal to stabilize after the start of cloud generation (droplet and
 5 memory effects in the sampling line).

6



1
 2 Figure 3: Time profiles of (a and a') O/C, OM/OC and H/C ratios (with the measurement
 3 uncertainty as determined by Aiken et al. (2008)), and (b and b') particle density for diphasic
 4 (left panel) and triphasic (right panel) experiments. Blue areas indicate cloud events.

5



1
 2 Figure 4: SOA chemical composition measured by an HR-ToF-AMS during a triphasic
 3 experiment (T280113) (a) before, (b) during and (c) 30 minutes after a cloud event. Right
 4 panels: mass spectra of dried aerosol averaged over 10 minutes (organic fragments are in green,
 5 nitrate fragments in blue and ammonium fragments in orange); Left panels: dried aerosol mass
 6 size distributions.

7

8